

## Ballistic Graphene Josephson Junctions from the Short to the Long Junction Regimes

I. V. Borzenets,<sup>1,\*</sup> F. Amet,<sup>2</sup> C. T. Ke,<sup>3</sup> A. W. Draelos,<sup>3</sup> M. T. Wei,<sup>3</sup> A. Seredinski,<sup>3</sup> K. Watanabe,<sup>4</sup> T. Taniguchi,<sup>4</sup> Y. Bomze,<sup>3</sup> M. Yamamoto,<sup>5</sup> S. Tarucha,<sup>1,6</sup> and G. Finkelstein<sup>3</sup>

<sup>1</sup>*Department of Applied Physics, University of Tokyo, Bunkyo-ku, Tokyo 113-8656, Japan*

<sup>2</sup>*Department of Physics and Astronomy, Appalachian State University, Boone, North Carolina 28607, USA*

<sup>3</sup>*Department of Physics, Duke University, Durham, North Carolina 27708, USA*

<sup>4</sup>*Advanced Materials Laboratory, National Institute for Materials Science, Tsukuba 305-0044, Japan*

<sup>5</sup>*PRESTO, JST, Kawaguchi-shi, Saitama 332-0012, Japan*

<sup>6</sup>*Center for Emergent Matter Science (CEMS), RIKEN, Wako-shi, Saitama 351-0198, Japan*

(Received 13 June 2016; published 2 December 2016)

We investigate the critical current  $I_C$  of ballistic Josephson junctions made of encapsulated graphene–boron-nitride heterostructures. We observe a crossover from the short to the long junction regimes as the length of the device increases. In long ballistic junctions,  $I_C$  is found to scale as  $\propto \exp(-k_B T/\delta E)$ . The extracted energies  $\delta E$  are independent of the carrier density and proportional to the level spacing of the ballistic cavity. As  $T \rightarrow 0$  the critical current of a long (or short) junction saturates at a level determined by the product of  $\delta E$  (or  $\Delta$ ) and the number of the junction’s transversal modes.

DOI: 10.1103/PhysRevLett.117.237002

Encapsulated graphene–boron-nitride heterostructures emerged in the past year as a medium of choice for studying proximity-induced superconductivity in the ultraclean limit [1–4]. These junctions support the ballistic propagation of superconducting currents across micron-scale graphene channels, and their critical current is gate-tunable across several orders of magnitude. In these devices, a rich phenomenology arises from the interplay of superconductivity with ballistic transport [1], cyclotron motion [2], and even the quantum Hall effect at high magnetic field [4].

In a superconductor-normal metal-superconductor (SNS) junction, single particles in the normal region cannot enter the superconductor and therefore experience Andreev reflections at each S-N interface. This results in Andreev bound states (ABS), which are capable of carrying superconducting current across the normal region. In long ballistic junctions, the energy spectrum of the ABS is quantized with a level spacing of  $E_0 = \pi \hbar v_F/L$ , where  $L$  is the junction length and  $v_F$  the Fermi velocity [5–9]. The energy of ABS cannot exceed the superconducting gap  $\Delta$ , so in the short junction regime,  $L \lesssim \xi \equiv \hbar v_F/\Delta$ , only a single ABS remains.

In this work we study several ballistic junctions of different length and demonstrate that the temperature dependence of the critical current dramatically differs in the long and short regimes. For long junctions, we observe an exponential scaling of the current through the junction  $I_C \propto \exp(-k_B T/\delta E)$ , where  $\delta E \approx \hbar v_F/2\pi L$  [5,6,10,11]. Note that in graphene  $v_F$  is a constant, and  $\delta E$  is expected to be independent of the carrier density or the mobility (as long as the junction remains ballistic.) For comparison, in a short junction we observe a different scaling, as expressed in Eq. (1), in agreement with the theory [12–14].

Our graphene layers are exfoliated from Kish graphite and encapsulated in hexagonal boron-nitride (hBN) using

the “pick-up” method [15]. Heating beyond 250 °C causes bubbles of trapped adsorbates to migrate towards the edges of the graphene mesa, effectively cleaning it. The edges of the graphene flake are exposed by etching through the hBN-graphene-hBN stack with a  $\text{CHF}_3/\text{O}_2$  plasma (flow rates 40/6 sccm) at 1 Pa and 60 W power. The etching time varies depending on the thickness of the top hBN layer. We use dc magnetron sputtering to form molybdenum-rhenium alloy contacts (50/50 wt %), with a measured superconducting gap  $\Delta_0 \approx 1.2$  meV [Fig. 1(b)]. These contacts are 100–120 nm thick and are deposited at a rate of  $\sim 50$  nm/min (with a pressure of 2 mTorr and a power of 160 W [4]). In this work we studied seven Josephson junctions with lengths ranging from 200 nm to 2000 nm. Device dimensions are listed in the Supplemental Material [16]. Junction A is found to be in the short regime, junctions B and E are intermediate, while junctions C, D, F, and G are in the long regime. Below we present primarily the data measured on four junctions A–D ( $L = 200$  nm, 400 nm, 1  $\mu\text{m}$ , and 2  $\mu\text{m}$ ) fabricated on the same flake.

The junctions are measured in a four-terminal setup with the carrier density in graphene being controlled by a gate voltage,  $V_G$ . Figure 1 presents a map of the differential resistance  $dV/dI(V_G, I)$ , measured on junction A at  $T = 1.5$  K. The dark region of vanishing resistance indicates a supercurrent, which persists at all values of  $V_G$ . As the current is swept from the negative to the positive values, the transition from the normal to the superconducting state is seen at negative bias when  $|I| = I_R$  (the retrapping current.) The transition from the superconducting back to the normal state happens at positive bias when  $I = I_S$ . As commonly observed in graphene Josephson junctions, at low temperatures the samples exhibit hysteresis,  $I_S \gtrsim I_R$  [22–27], which could be attributed to either underdamped

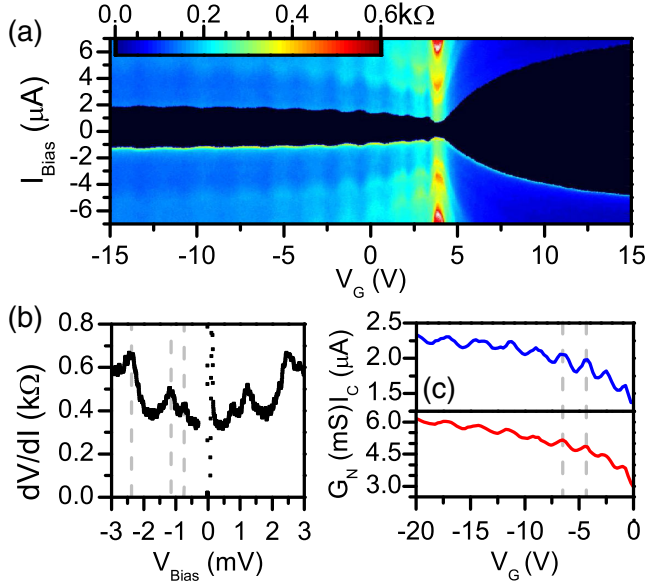


FIG. 1. (a) Map of differential resistance vs current  $I$  and gate voltage  $V_G$ . The data are shown for junction A and taken at a temperature  $T = 1.5$  K. The superconducting region of zero resistance can be observed around  $I = 0$ . The current through the junction is swept from negative to positive; therefore, the transition at the negative  $I$  corresponds to the retrapping current  $I_R$ , while the transition at the positive  $I$  corresponds to the switching current  $I_S$ . (b) Differential resistance vs bias voltage ( $V_B$ ) for junction A taken at the Dirac point. Several multiple Andreev reflection (MAR) peaks are observed:  $2\Delta$ ,  $\Delta$ ,  $2/3\Delta$ ; with  $\Delta \approx 1.2$  meV. (c) The critical current  $I_C$  (top) and the normal conductance of the junction (bottom) plotted vs gate voltage  $V_G$  in the hole conduction regime. Both quantities demonstrate Fabry-Perot oscillations and are roughly proportional to each other.

junction dynamics [8,25], or to the self-heating by the retrapping current [27,28]. As discussed in the Supplemental Material, the second scenario is more likely for most of the range studied here. Based on the

measurements of the switching statistics [16,29–31], in the following we will use the switching current to represent the true critical current of the junction,  $I_C$ .

In the hole-doped regime, the reflections of ballistic charge carriers from the  $n$ -doped contact interfaces yield the quantum (“Fabry-Perot”) interference. A very similar oscillation pattern could be observed in the dependence of both the normal conductance  $G_N$  and the critical current  $I_C$  on gate voltage  $V_G$  [Fig. 1(c)] [1,2,4]. Oscillations in normal resistance  $R_N$  are also observed as a function of bias voltage  $V_B$  [Fig. 4(a), inset] [2,4,32,33].

The critical current  $I_C$  is observed to rapidly decrease with temperature; however, the functional form of  $I_C(T)$  strongly depends on the length of the junction. Figure 2 shows the evolution of  $I_C(T)$  from the short to the long regime. Each panel shows data taken for several values of  $V_G$ , which from here on is measured relative to the Dirac point. The shortest junction [Fig. 2(a)] can only support a single ABS; in this regime, the current is

$$I_C(T, \phi) \propto \frac{e\Delta}{R_N} \frac{\sin \phi}{\sqrt{1 - \tau \sin^2 \phi/2}} \tanh \left( \frac{\Delta}{2k_B T} \sqrt{1 - \tau \sin^2 \phi/2} \right), \quad (1)$$

where  $\tau$  is the transmission coefficient of the S-N interface and  $R_N$  the normal state resistance. For a given  $T$ , this expression should be maximized over  $\phi$  to determine  $I_C(T)$  [12–14]. Moreover, at higher temperatures the superconducting gap will be suppressed; we approximate the temperature dependence of the gap as  $\Delta(T) \approx \Delta_0 \sqrt{1 - (T/T_C)^2}$ , where  $\Delta_0$  is the gap for  $T \rightarrow 0$ , and  $T_C$  is the critical temperature [8,34,35]. Taking the temperature-dependent expression, we fit  $I_C(T)$  for junction A using the value  $\Delta_0 = 1.2$  meV extracted from

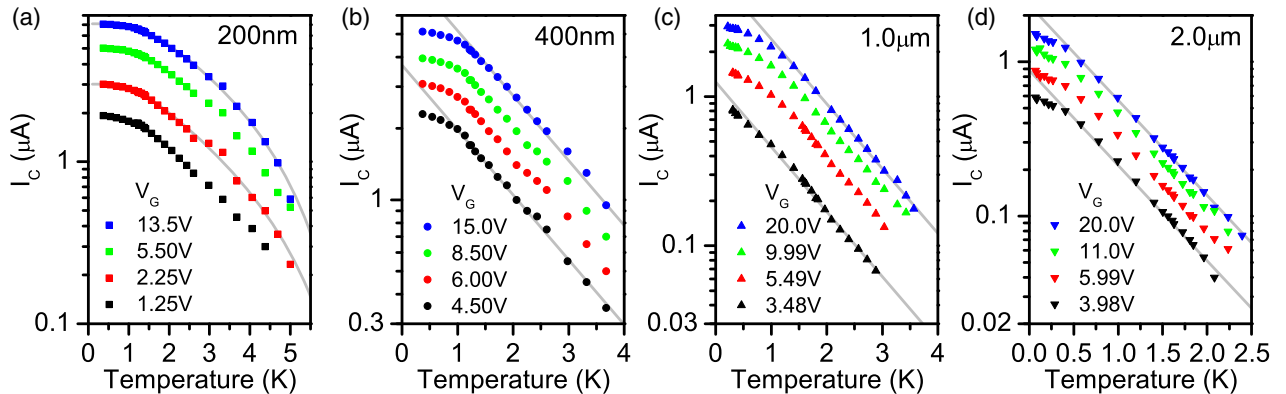


FIG. 2. Critical currents  $I_C$  plotted on a semi-log scale vs temperature  $T$  for junctions A–D.  $I_C$  at several gate voltages are presented for each junction; the values of  $V_G$  are shown relative to the Dirac point. (a) The data for the shortest junction, A ( $L = 200$  nm). The gray lines are fitted according to Eq. (1), using the superconducting gap  $\Delta$  extracted in Fig. 1(b). (b)–(d)  $I_C$  vs  $T$  for junctions B–D, respectively (see Supplemental Material [16] for junctions E, F, G). The slope of  $\log(I_C)$  vs  $T$  is independent of  $V_G$ . In the case of long ballistic graphene junctions, the inverse slope  $\delta E$  is expected to be independent of the carrier density and inversely proportional to  $L$ .

multiple Andreev reflections measurements. The fit is in excellent agreement with the data [Fig. 2(a)].

The transmission coefficient  $\tau$  extracted from the fit is plotted in the inset of Fig. 3 as a function of the gate voltage. We can also estimate the transmission coefficient via an alternative method, by comparing the junction normal conductance  $G_N$  to the ballistic limit of conductance  $G_0 = Ne^2/h$ , where  $N = 4\sqrt{(n/\pi)W}$  is the number of transversal modes and  $n = V_G C_G/e$  is the carrier density.  $\tau$  estimated as  $G_N/G_0$  is shown in blue in the inset of Fig. 3. Both methods provide consistent results, with  $\tau$  in junction A reaching 90% at high densities. Furthermore, we find that the normal conductance of all junctions is very close to the ballistic limit. Figure 3(a) compares the normal conductance of junctions A–D normalized by the junction’s width (in fact, junctions A–C have the same widths). All four curves are very close to each other and approach the ballistic limit for positive gate voltages (dashed line). This result indicates two important facts: (i) the contacts of all junctions are highly

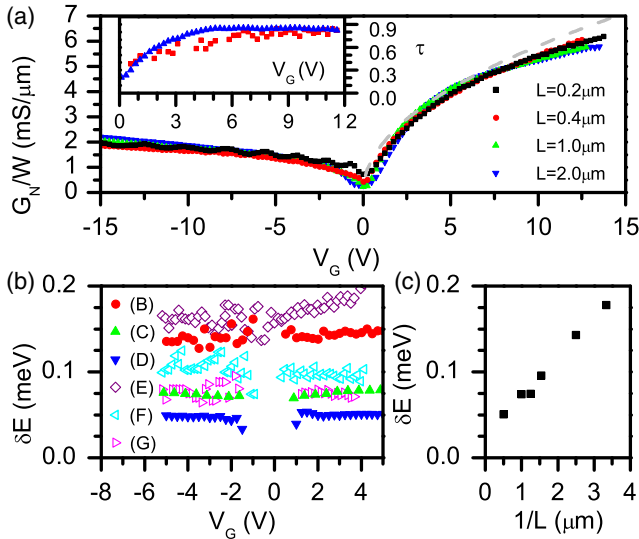


FIG. 3. (a) Normal conductance of junctions A–D normalized by the width of the junctions  $G_N/W$ . Even though the device lengths are different by up to a factor of 10, the three curves are very close to each other, thus proving the ballistic nature of these junctions. At positive  $V_G$ ,  $G_N$  of all junctions is found to approach  $G_0 = Ne^2/h$  (gray dashed line), indicating consistently high contact transparency for  $n$  doping in these devices. Inset: Transmission coefficient  $\tau$  of junction A.  $\tau$  is calculated via two methods: comparing the normal conductance  $G_N$  to the ballistic limit  $G_0 = Ne^2/h$  (blue), and fitting the critical current  $I_C$  vs temperature  $T$  (red). Both methods provide consistent results and indicate high contact transparency for  $n$  doping. (b) Energy  $\delta E$  extracted from the slope of  $\log(I_C)$  vs  $T$  for junctions (B–G). As expected in the long junction regime,  $\delta E$  depends only on device length  $L$  and is almost density independent through both the electron and hole doping. (c) Length dependence of  $\delta E$  showing a linear  $1/L$  dependence.

transparent on the  $n$ -doped side and (ii) the junctions’ conductances do not depend on length, confirming their ballistic nature.

We now return to the critical current measured in the longer junctions B–D. In Figs. 2(b)–2(d),  $I_C$  is plotted on a semilogarithmic scale and clearly shows exponential dependence at high temperatures  $T$  [over an order of magnitude in panels (c) and (d)]. This is consistent with the expected long junction behavior  $I_C \propto \exp(-k_B T/\delta E)$  [5–7,9–11] and allows us to extract the energy scale  $\delta E$ . The temperature dependence eventually saturates at low temperatures, when  $k_B T$  becomes comparable to  $\delta E$ .

Figure 3(b) shows that for a given device  $\delta E(V_G)$  remains roughly constant as a function of  $V_G$  for both electron and hole doping, as expected in the long ballistic regime.  $\delta E$  is on the order of 0.05 meV for the longest device, junction D, and goes up to  $\sim 0.2$  meV for junction E. While  $\delta E$  is consistent with the expected value of  $\hbar v_F/2\pi L$  for junction D, it is suppressed for shorter junctions. As the devices are ballistic, the suppression of  $\delta E$  cannot be explained by the effective lengthening of the carrier path due to diffusion.

To explain the suppressed  $\delta E$ , we observe that the previous discussion of the long junctions neglected the coherence length  $\xi$  compared to  $L$ . Taking  $\xi$  into account suppresses the level spacing, which becomes  $E_0 = \pi\hbar v_F/(L + \xi)$  [36]. While the general expression for  $I_C(T)$  in the  $L \approx \xi$  regime is not known, numerical simulations show that it still roughly follows the  $\propto \exp(-k_B T/\delta E)$  dependence, with  $\delta E$  suppressed by a factor of  $\sim 2$  compared to the estimate that neglects  $\xi$  [Fig. 3(b) in Ref. [34]]. In our case,  $\xi \approx 550$  nm, which explains the suppressed  $\delta E$  in the intermediate regime (junctions B, E). Eventually, the junction transitions to the short regime, where the exponential dependence no longer holds.

We now turn to the saturation of  $I_C$  in the low temperature limit:  $k_B T \ll \Delta_0$  for a short junction, or  $k_B T \ll \delta E$  for a long junction. In the long ballistic junction regime, the  $T = 0$  critical current is expected to be on the order of  $e\delta E/h$  per transversal mode [7,9,37]. Figure 4(b) shows the ratio  $hI_C/Ne\delta E$  as a function of the gate voltage. Strikingly, the curves for the four junctions are very close to each other and converge to a constant level of  $\approx 1$  at high gate voltage, where the graphene-MoRe interfaces are highly transparent. (See Supplemental Material [16] for data on additional devices.) Similarly, the  $T = 0$  critical current per mode is expected to be  $\sim e\Delta_0/h$  in an ideal short junction [8,9]. Figure 4(a) plots the ratio  $hI_C/Ne\Delta_0$  for junction A, which indeed saturates at high gate voltage, although its value  $\approx 0.3$  is significantly smaller than  $\sim 2$  predicted by theory of Ref. [38]. Previous works have observed similar deviations from theory [2]. The mechanism for such suppression is unclear and cannot be explained by environmental damping effects, nor the effect

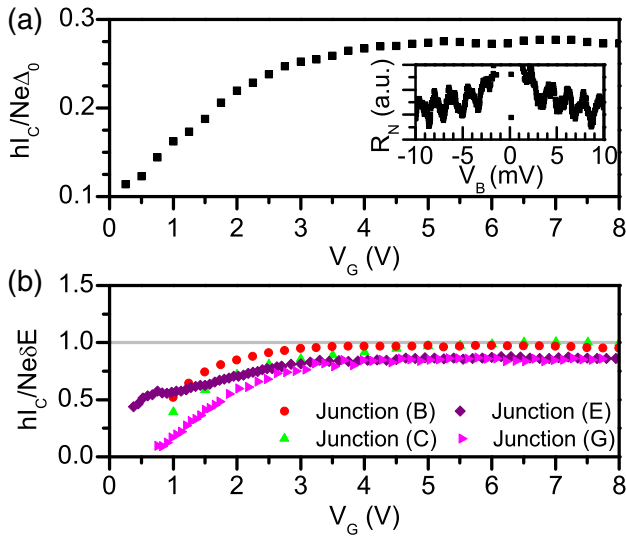


FIG. 4. (a) The ratio  $hI_C/Ne\Delta_0$  measured on junction A at  $T = 300$  mK as a function of  $V_G$ . The number of modes  $N$  is  $W(4\sqrt{n/\pi})$ , where  $n$  is the carrier density as determined from  $V_G$ . As the gate voltage increases and the transmission of the graphene-MoRe interfaces approaches 1, the plotted ratio saturates. Inset: Differential conductance vs bias voltage  $V_B$  for the 650 nm long junction F, gated to the  $p$ -doped regime ( $V_G = -4.2$  V). The period of the Fabry-Perot oscillations yields the level spacing,  $E_0 \approx 2$  meV, which is consistent with the expected  $E_0 = 2\pi^2\delta E$  ( $\delta E \approx 0.1$  meV for this junction.) (b) The ratio  $hI_C/Ne\delta E$  for junctions in the long regime (B,C,E,G), measured as a function of  $V_G$  at 60 mK. (See Supplemental Material [16] for junction F. Junction D does not yet saturate at the base temperature.) At higher  $V_G$  the ratio converges toward a constant value in all junctions.

of imperfect transmission [16]. [Note: as there are currently no graphene-specific theoretical works predicting the ratio  $hI_C/Ne\delta E$  in the long regime, it is unclear whether the value of  $\sim 1$  observed in Fig. 4(b) is coincidental.]

The ratio  $hI_C/Ne\delta E$  is significantly reduced close to charge neutrality. This suppression most likely arises from the  $V_G$  dependence of the transmission coefficient  $\tau$  of the superconductor-graphene interface. We extract the contact transparency from the junction normal resistance as  $h/Ne^2R_N$  and find that while  $\tau$  is close to 1 at high densities, it does get significantly suppressed close to the charge neutrality point. Considering this suppression allows us to partially account for the reduced  $hI_C/Ne\delta E$  ratio (see Supplemental Material [16]).

In conclusion, we studied the nature of the critical current in several ballistic superconductor-graphene-superconductor junctions. We find that in the short junction regime,  $L \ll \xi$ , the critical current follows Eq. (1), while in the intermediate and long junctions  $I_C$  is  $\propto e^{-k_B T/\delta E}$ . The slope of  $\log I_C$  vs  $T$  dependence allows us to extract the energy scale  $\delta E$ , which depends on the junction length but not the gate voltage  $V_G$ . While consistent for very long

junctions  $L \gg \xi$ , the values of  $\delta E$  for intermediate devices  $L \sim \xi$  are smaller than those naively estimated from the junction lengths. We attribute this suppression to the finite coherence length. Finally, we show that at the lowest temperature,  $I_C$  saturates at a level determined by the product of  $\Delta_0$  or  $\delta E$  (depending on the regime), and the number of transversal modes across the junction width. Our observations demonstrate the universality of the critical current in several regimes relevant to most hybrid superconductor-encapsulated graphene devices.

I. V. B. and M. Y. acknowledge the Canon Foundation. F. A. acknowledges the ARO Grant No. W911NF-14-1-0349. M. T. W. and A. S. were supported by ARO Grant No. W911NF-16-1-0122. A. W. D. was supported by the NSF graduate research fellowship DGF1106401. Low-temperature measurements performed by C. T. K. and G. F. were supported by the Division of Materials Sciences and Engineering, Office of Basic Energy Sciences, U.S. Department of Energy, under Award No. DE-SC 0002765. This work was performed in part at the Duke University Shared Materials Instrumentation Facility (SMIF), a member of the North Carolina Research Triangle Nanotechnology Network (RTNN), which is supported by the National Science Foundation (Grant No. ECCS-1542015) as part of the National Nanotechnology Coordinated Infrastructure (NNCI). M. Y. acknowledges support from JSPS KAKENHI Grant No. JP25107003. K. W. and T. T. acknowledge support from JSPS KAKENHI Grant No. JP15K21722 and the Elemental Strategy Initiative conducted by the MEXT, Japan. T. T. acknowledges support from JSPS Grant-in-Aid for Scientific Research A (No. 26248061) and JSPS Innovative Areas “Nano Informatics” (No. 25106006). M. Y. and S. T. acknowledge support by Grant-in-Aid for Scientific Research S (No. 26220710), and Grant-in-Aid for Scientific Research A (No. 26247050, 16H02204). We would like to thank Konstantin Matveev for fruitful discussions.

\*Corresponding author.

ivan@meso.t.u-tokyo.ac.jp

- [1] V. E. Calado, S. Goswami, G. Nanda, M. Diez, A. R. Akhmerov, K. Watanabe, T. Taniguchi, T. M. Klapwijk, and L. M. K. Vandersypen, *Nat. Nanotechnol.* **10**, 761 (2015).
- [2] M. Ben Shalom, M. J. Zhu, V. I. Fal’ko, A. Mishchenko, A. V. Kretinin, K. S. Novoselov, C. R. Woods, K. Watanabe, T. Taniguchi, A. K. Geim, and J. R. Prance, *Nat. Phys.* **12**, 318 (2016).
- [3] M. T. Allen, O. Shtanko, I. C. Fulga, J. I. J. Wang, D. Nurgaliev, K. Watanabe, T. Taniguchi, A. R. Akhmerov, P. Jarillo-Herrero, L. S. Levitov, and A. Yacoby, *Nat. Phys.* **12**, 128 (2016).

- [4] F. Amet, C. T. Ke, I. V. Borzenets, Y. Wang, K. Watanabe, T. Taniguchi, R. S. Deacon, M. Yamamoto, Y. Bomze, S. Tarucha, and Finkelstein, *Science* **352**, 966 (2016).
- [5] I. O. Kulik, *Sov. Phys. JETP* **30**, 944 (1970).
- [6] J. Bardeen and J. L. Johnson, *Phys. Rev. B* **5**, 72 (1972).
- [7] A. V. Svidzinskii, *Spacially-Inhomogeneous Problems of Theory of Superconductivity* (Nauka, Moscow, 1982).
- [8] M. Tinkham, *Introduction To Superconductivity* (McGraw-Hill, New York, 1996).
- [9] A. A. Golubov, M. Yu. Kupriyanov, and E. Ilichev, *Rev. Mod. Phys.* **76**, 411 (2004).
- [10] A. V. Svidzinsky, T. N. Antsygina, and E. N. Bratus, *Sov. Phys. JETP* **3**, 860 (1972).
- [11] A. V. Svidzinsky, T. N. Antsygina, and E. N. Bratus, *J. Low Temp. Phys.* **10**, 131 (1973).
- [12] C. W. J. Beenakker, *Transport Phenomena in Mesoscopic Systems* (Springer, Berlin, 1992), p. 235.
- [13] C. W. J. Beenakker and H. van Houten, *Phys. Rev. Lett.* **66**, 3056 (1991).
- [14] G.-H. Lee, S. Kim, S.-H. Jhi, and H.-J. Lee, *Nat. Commun.* **6**, 6181 (2015).
- [15] L. Wang, I. Meric, P. Y. Huang, Q. Gao, Y. Gao, H. Tran, T. Taniguchi, K. Watanabe, L. M. Campos, D. A. Muller, J. Guo, P. Kim, J. Hone, K. L. Shepard, and C. R. Dean, *Science* **342**, 614 (2013).
- [16] See Supplemental Material at <http://link.aps.org/supplemental/10.1103/PhysRevLett.117.237002> for data on additional devices, switching statistics, and the effect of transmission, which includes Refs. [17–21].
- [17] T. A. Fulton and L. N. Dunkleberger, *Phys. Rev. B* **9**, 4760 (1974).
- [18] J. Clarke, E. A. Cleland, H. M. Devoret, D. Esteve, and M. J. Martinis, *Science* **239**, 992 (1988).
- [19] M. Yu. Kupriyanov and V. F. Lukichev, *Zh. Eksp. Teor. Fiz.* **94**, 139 (1988).
- [20] Y. Luh, *Acta Phys. Sin.* **21**, 75 (1965); H. Shiba, *Prog. Theor. Phys.* **40**, 435 (1968); A. I. Rusinov, *Sov. Phys. JETP* **29**, 1101 (1969).
- [21] G. Eilenberger, *Z. Phys.* **214**, 195 (1968).
- [22] H. B. Heersche, P. Jarillo-Herrero, J. B. Oostinga, L. M. K. Vandersypen, and A. F. Morpurgo, *Nature (London)* **446**, 56 (2007).
- [23] X. Du, I. Skachko, and E. Y. Andrei, *Phys. Rev. B* **77**, 184507 (2008).
- [24] C. Ojeda-Aristizabal, M. Ferrier, S. Guéron, and H. Bouchiat, *Phys. Rev. B* **79**, 165436 (2009).
- [25] I. V. Borzenets, U. C. Coskun, S. J. Jones, and G. Finkelstein, *Phys. Rev. Lett.* **107**, 137005 (2011).
- [26] I. V. Borzenets, U. C. Coskun, S. J. Jones, and G. Finkelstein, *IEEE Trans. Appl. Supercond.* **22**, 1800104 (2012).
- [27] I. V. Borzenets, U. C. Coskun, H. T. Mebrahtu, Yu. V. Bomze, A. I. Smirnov, and G. Finkelstein, *Phys. Rev. Lett.* **111**, 027001 (2013).
- [28] H. Courtois, M. Meschke, J. T. Peltonen, and J. P. Pekola, *Phys. Rev. Lett.* **101**, 067002 (2008).
- [29] U. C. Coskun, M. Brenner, T. Hymel, V. Vakaryuk, A. Levchenko, and A. Bezryadin, *Phys. Rev. Lett.* **108**, 097003 (2012).
- [30] G.-H. Lee, D. Jeong, J. H. Choi, Y.-J. Doh, and H.-J. Lee, *Phys. Rev. Lett.* **107**, 146605 (2011).
- [31] C. T. Ke, I. V. Borzenets, A. W. Draelos, F. Amet, Yu. Bomze, G. Jones, M. Craciun, S. Russo, M. Yamamoto, S. Tarucha, and G. Finkelstein, *Nano Lett.* **16**, 4788 (2016).
- [32] A. F. Young and P. Kim, *Nat. Phys.* **5**, 222 (2009).
- [33] P. Rickhaus, R. Maurand, M.-H. Liu, M. Weiss, K. Richter, and C. Schenberger, *Nat. Commun.* **4**, 2342 (2013).
- [34] I. Hagymasi, A. Kormanyos, and J. Cserti, *Phys. Rev. B* **82**, 134516 (2010).
- [35] R. Dougherty and J. D. Kimel, *Superconductivity Revisited* (CRC Press, London 2013).
- [36] P. F. Bagwell, *Phys. Rev. B* **46**, 12573 (1992).
- [37] C. Ishii, *Prog. Theor. Phys.* **44**, 1525 (1970).
- [38] M. Titov and C. W. J. Beenakker, *Phys. Rev. B* **74**, 041401(R) (2006).